



OPEN

In situ TEM Observation of Resistance Switching in Titanate Based Device

Yang Yang, Weiming Lü, Yuan Yao, Jirong Sun, Changzhi Gu, Lin Gu, Yanguo Wang, Xiaofeng Duan & Richeng Yu

Beijing National Laboratory of Condensed Matter Physics, Institute of Physics, Chinese Academy of Sciences, Beijing 100190, P. R. China.

After decades of efforts, the research on resistance switching (RS) behavior in transition metal oxides has shifted to the stage of verifying the proposed models by direct experimental evidences. In this paper, RS behavior and oxygen content variation of $\text{La}_{0.85}\text{Sr}_{0.15}\text{TiO}_3/\text{SrTiO}_3:\text{Nb}$ (LSTO/STON) were investigated by *in situ* transmission electron microscopy observation and *in situ* electron energy loss spectrum characterization under external electric field. The oxygen content fluctuation adjusted by applied bias has been investigated and the observed results imply the conductive channels should be formed by the oxygen vacancy at the Pt/LSTO interface. Moreover, *in situ* TEM characterization displays the advantage - to reveal the origin of various RS behaviors.

Coming up against the challenge of speed and scaling, the conventional Flash memory has reached its limit in application¹. To meet the requirement for higher speed and larger capacity from the information technology, the next-generation non-volatile memories have been arising. Compared with these candidates of ferroelectric random access memory (FRAM)², magnetoresistive RAM (MRAM)³ and phase-change RAM (PRAM)⁴, the resistance random-access memory (RRAM) possesses the distinct advantage because of its simple fabrication process, fast read and write speed, high storage density and multi-level storage application. So RRAM is becoming one of the rapid development fields both in semiconductor engineering and scientific researches⁵⁻⁹.

The principle of most RRAM is based on the “resistance switching” (RS) phenomenon⁷, of which the resistance of the metal-insulator-metal (MIM) structured device could be repeatedly set to different levels by external electric field and these resistance levels, usually showing bistability as high resistance state (HRS) and low resistance state (LRS) corresponding to the binary data storage of 0 and 1, respectively, could maintain the last state when electric field is removed. Although the RS phenomenon was pioneered in the early 1960s¹⁰⁻¹², the application for memory device was realized as electric pulse induced resistance switching in 2000¹³.

Besides the fabrication technique of RRAM devices, the essence of RS behavior is still a research focus. During the last decade, many mechanisms, such as conductive filaments (CF)⁹, metal ion migration^{14,15}, interface barrier change¹⁶⁻¹⁸, redox reaction⁵, Joule heat effect¹⁹, polaron ordering and melting model²⁰ were proposed as well as various experimental results. According to those models, three significant conditions must be satisfied to realize RS. First, there must be some intrinsic physical changes evoked by the stimulation of external electric field to convert the device from one state to another, sometimes among multiple states²¹. Second, these states should have distinctively different electric conductivities, corresponding to the HRS and LRS. Third, these variations cannot be recovered unless proper external electric field is applied. Only with this property could the resistance states be engineered artificially and the simplex metal-to-insulator transition in oxides²² is excluded.

The detail of the first condition is the major bone of contention among those models because various materials are employed in the MIM stacks. It is proposed that the ions of oxidable metal (Ag or Cu) of the anode in MIM stacks could migrate through the insulator, accumulate at the cathode and form the CF, whose dissolving and reforming result in the RS behavior. Such a model was verified by *in situ* TEM observation and elemental analysis recently^{14,15}. On the contrary, another assumption proposes that RS behavior originates from the local intrinsic (structure or composition) change of the insulate layer of the MIM. Kwon, et al.²³ observed directly that low resistance Ti_4O_7 (Magnéli) phase emerged in TiO_2 film sandwiched by Pt electrodes and vanished during the transition from the LR to HR state. So the structure change of TiO_2 should be responsible for the RS behavior. In Yoo's report²⁴, the changes of grain boundaries in NiO were regarded as the origin of RS properties. Xu et al.¹⁸ announced that generation of oxygen ions (or oxygen vacancies) changed the height and width of Schottky barrier

Received
12 August 2013
Accepted
6 January 2014
Published
27 January 2014

Correspondence and requests for materials should be addressed to R.C.Y. (rcyu@aphy.iphy.ac.cn)

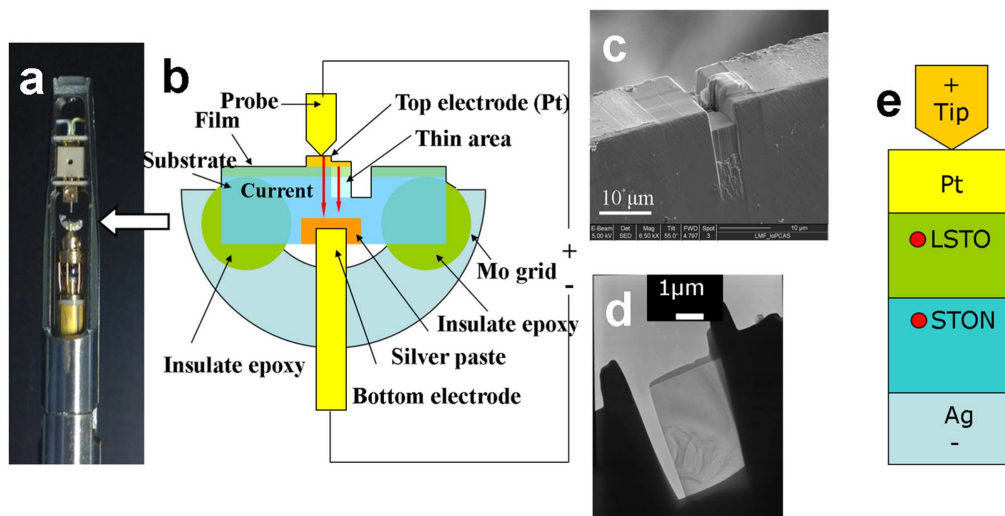


Figure 1 | Schematic of the *in situ* TEM experimental set-up. (a), The image of the top of the holder for *in situ* TEM characterization. (b), Schematic diagram of *in situ* test. (c), The scanning electron micrograph of the TEM sample. (d), The TEM micrograph of the sample. (e), Schematic diagram of the *in situ* test and the position where the EELS was acquired.

at the interface and caused the different conductivities. These literatures related the intrinsic change to the local oxygen content variation, such as the oxygen vacancy which is one of the most fundamental defects and indeed has a critical impact on the electrical property^{25,26}. However, direct experimental evidences of the relationship between oxygen content and RS are rare because the detection of local change of oxygen vacancies, including the dynamic process, requires high spatial and elemental resolutions.

Recently, the state-of-the-art *in situ* transmission electron microscopy (TEM) has been developed to study the microstructures and physical properties of materials simultaneously²⁷, which have promoted the research of RS materials^{14,15,20,23}. Here, we report the investigation of RS behavior and oxygen content variation of Pt/La_{0.85}Sr_{0.15}TiO₃/SrTiO₃:Nb/Au (Pt/LSTO/STON/Au) device with *in situ* TEM observation and *in situ* electron energy loss spectroscopy (EELS) analysis and reveal the relationship between the oxygen stoichiometry variation and RS behavior. The experimental results support the barrier change mechanism, which is caused by CF involving the oxygen vacancies at the Schottky interface.

Results

To realize an *in situ* observation of TEM, we made a tiny fine structure based on the traditional cross-section TEM sample preparation and focused ion beam (FIB) technique (Fig. 1). Although SrTiO₃ is a simple cubic perovskite as a model band insulator²⁵, the Nb-doped SrTiO₃ (STON) is an important conductive ingredient of oxide

heterojunctions or homojunctions for both practical application and fundamental research²⁸. The structure of as prepared LSTO/STON interface is illustrated in Fig. 2. A high resolution TEM image and the corresponding electron diffraction pattern without splitting spots indicate the matched epitaxial growth of the films. It is hard to identify the STON substrate and the LSTO film in TEM image unless referring the EELS spectra of La-M₄, M₅ (Fig. 2b). The hysteresis I-V curve of the pristine bulk sample shown in Fig. 2c confirms the voltage pulse could switch the resistance properties between insulating and conducting states though the repeat is limited.

A longer “forming” time is necessary for the *in situ* TEM sample before the RS behavior is observed. No infiltration of Pt metal was detected in the LSTO film, so the metal CF model could be excluded and some intrinsic changes inside LSTO should trigger the RS behavior.

RS behavior was found by *in situ* I-V measurement after the “forming” process, as represented in Fig. 3, where four separated stages describe the RS procedure of one cycle. In the stages “1” and “4” of Fig. 3a, the sample stays at HRS, exhibiting nonlinear I-V behavior. Proper voltage results in linear I-V curve as LRS in the stages “2” and “3”. The resistance could be switched repeatedly for more than 8 times (Fig. 3b), and the resistance ratio between HRS and LRS ($R_{\text{HRS}}/R_{\text{LRS}}$) is about 220%. Because the instability of the tip-sample system, we did many experiments but could not get information for more than 15 cycles in each experiment, but during these cycles, the RS behaviors existed and were nearly the same. The

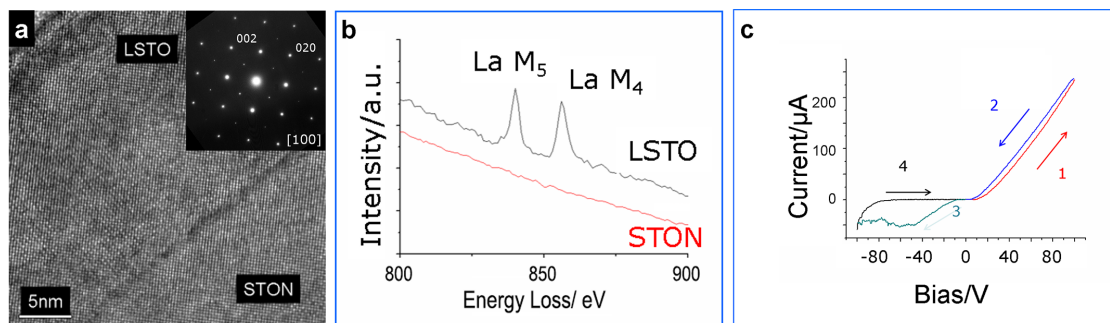


Figure 2 | Basic structure and I-V property of the sample. (a), High resolution TEM image of LSTO/STON, the inset is the electron diffraction pattern of the interface. (b), EELS of La in LSTO and STON. (c), The I-V curve of pristine bulk LSTO/STON samples. The voltage sweep sequence is showed by the arrows and numbers.

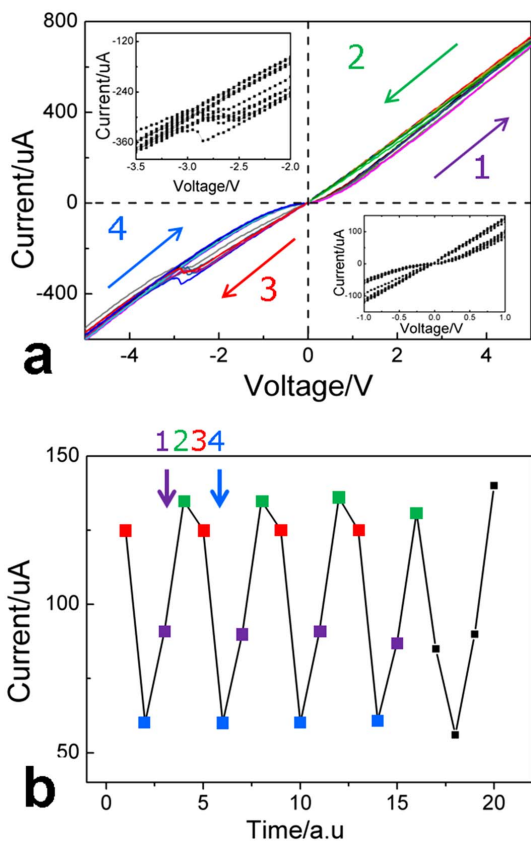


Figure 3 | Resistance switching in LSTO/STON device during the *in situ* TEM experiment. (a), I-V curve from -5 V to 5 V for five cycles, where the arrows and numbers indicate the sequence and the insets show the detail from -3.5 V to -2 V and from -1 V to 1 V, respectively. (b), The current variation under ± 1 V, where the numbers indicate the corresponding sequences in Fig. 3 a.

positive bias could only decrease the resistance while the negative one could only increase it, indicating that it is a typical bipolar switching phenomenon⁷. The I-V curve seems very similar to that of the pristine sample in Fig. 2c. The resistance change is not obvious in the positive bias region, compared with that in the negative case. A critical voltage for the resistance change could be identified as about -2.5 V to -3 V (the top-left inset of Fig. 3a) and the RS ratio is about 150% at 1 V (absolute value). During the RS behavior, no obvious morphology change of the sample was observed (see Fig. S1).

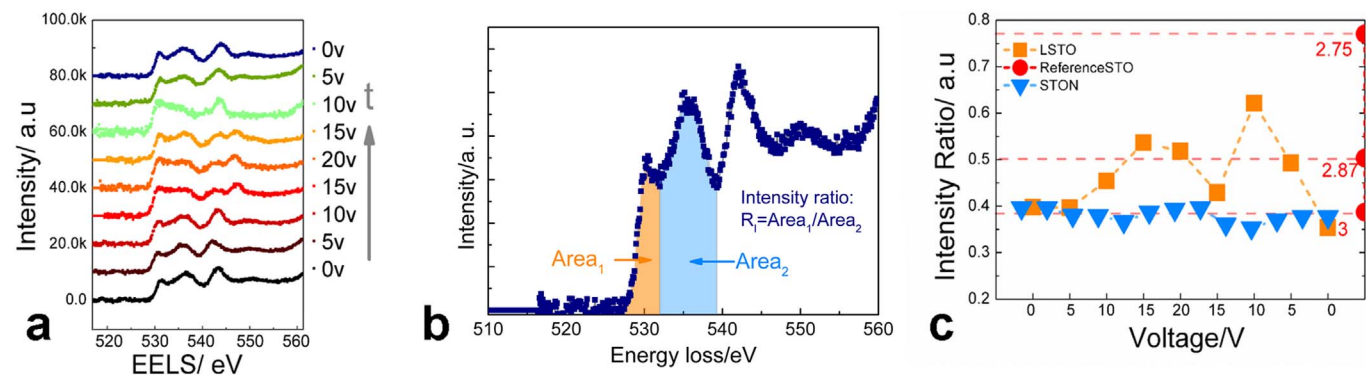


Figure 4 | The oxygen content fluctuation adjusted by applied bias in the “forming” process. (a), EELS of O-K edge under different voltages at “Interface”. (b), The method used to calculate the intensity ratio for estimating the oxygen concentration. c, The intensity ratio obtained from the EELS data of two positions in Fig. 4 a with the reference data calculated from reference 29 with the same method, the red numbers label the stoichiometric values x in SrTiO_x , and the gray arrow indicates the sequence of the experiments.

Although the atomic resolution image in our *in situ* experiments is hardly realized, we could still obtain the local elemental information by EELS characterization. Simultaneous with the observation, significant changes of oxygen content at the Pt/LSTO interface were also identified, as shown in Fig. 4 and Fig. 5. Under different voltages, the shape of the O-K EELS peaks changes regularly at the position of Pt/LSTO interface (labeled as LSTO), a 3 nm spot in Fig. 1e.

Discussion

EELS is very sensitive to the chemical environment of the atoms, therefore a little change of oxygen content would be reflected in the fine structure of O-K EELS^{29–31}. In the perovskite titanates, the O-K EELS including several peaks describes the transition of the electrons from the O 1s shell to unoccupied 2p orbit hybridizing strongly with metal 3d orbitals. For example, the first and second peaks of O-K EELS in Fig. 4b represent the Ti-O and Sr-O bonding, respectively³⁰. Due to the limit of resolution, we cannot discern more detailed but can compare our results quantitatively with the EELS data of the reference STO with definite stoichiometry²⁹. The first and second peaks of O-K edge were integrated respectively in the given energy range (Fig. 4b) and then the ratio of two integrated intensities was used to demarcate the oxygen vacancy variation. The ratios obtained from the *in situ* experimental data were plotted in Fig. 4c as well as the reference STO which was a benchmark to estimate the quantity of the oxygen content. The red dashed line in Fig. 4c presents the data from the reference STO and indicates that the ratio should increase as the oxygen content reduces (or the density of oxygen vacancy increases). Compared with the reference, the results from the *in situ* experiments demonstrate that the density of oxygen vacancy at Pt/LSTO interface increases when the voltage increases from 0 V to 20 V, implying that the oxygen vacancies are generated at the interface by electrochemical reactions under positive voltage during the “forming” process, similar to the reported CF formation process in TiO_2 ⁹ where the high voltage could accelerate the electrochemical reaction rate and increase the density of oxygen vacancy at the interface between the electrode and TiO_2 . The drop of intensity ratios is out of sync with the decrease of voltage and shows a little hysteresis when the voltage reduces from 20 V to 0 V, which may reflect the migration of oxygen vacancies from the interface of Pt/LSTO down towards the cathode. It should be noted that the intensity ratio under 15 V in the decreasing voltage process is out of trend due to unknown reasons at the moment. The oxygen content change is less than 8%, thus it may be not enough to cause the structural change in LSTO. The inconspicuous intensity ratio ripple of O-K EELS under same voltage at the point STON in Fig. 1e also supports that the electrochemical reaction induced oxygen vacancy fluctuation takes place mainly at the interface. Because “forming” process could not

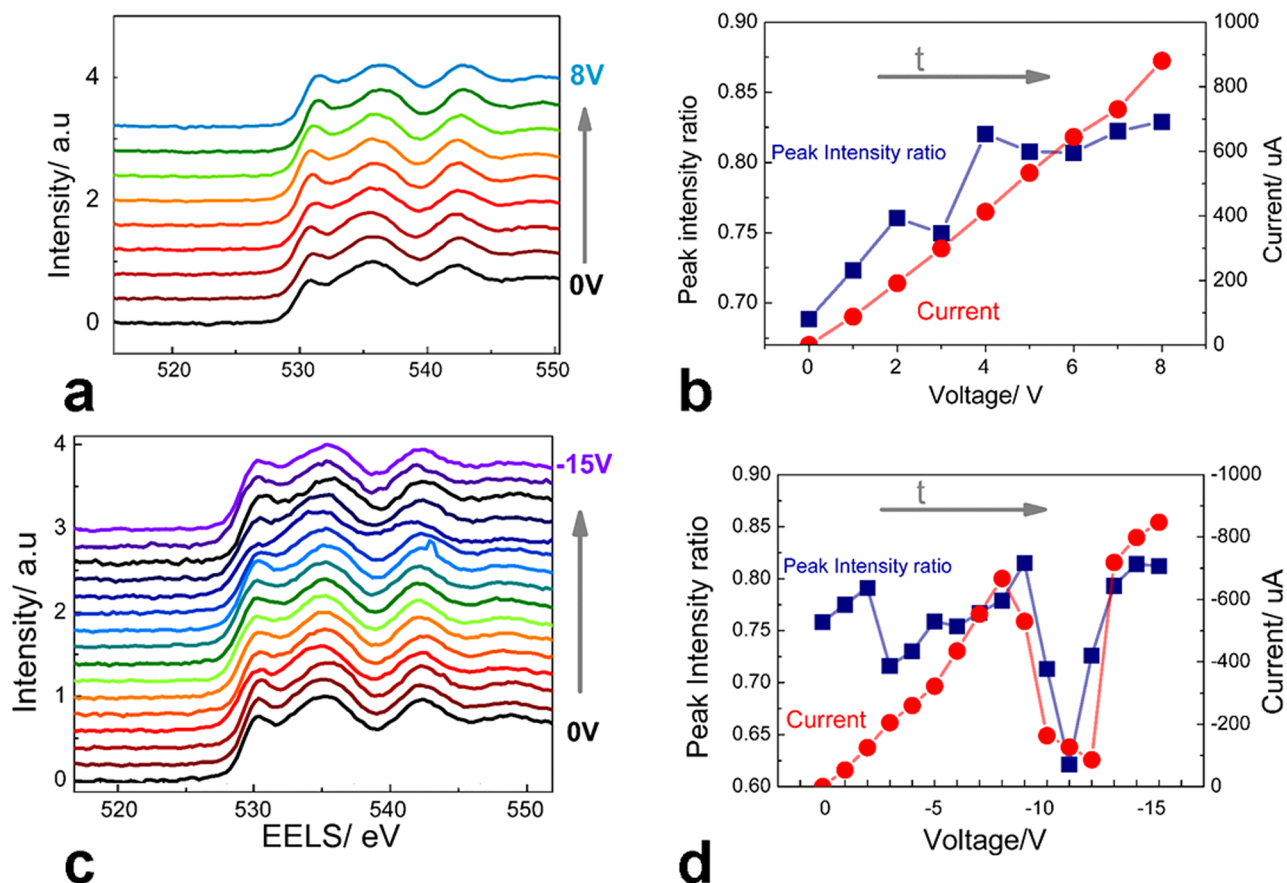


Figure 5 | O-K edge and the intensity ratio under voltages with corresponding current in the RS process. (a), (b) for the positive bias and c, d for the negative bias, respectively. The gray arrows indicate the sequence of the experiments.

reproduce once the “switching” process is achieved, we have only added the positive voltage in that time of experiment. And we recorded the information by adding a negative voltage to another sample, but no significant elemental change was found.

To investigate the relationship between the oxygen vacancy and the resistance state, the oxygen vacancy variations at the Pt/LSTO interface under different voltages in both LRS and HRS are presented in Fig. 5. The density of oxygen vacancy increases smoothly as positive bias increases (Fig. 5a and b), similar to stage 1 in Fig. 3a, while for the status like the stage 3 in Fig. 3a the drastic density loss of the oxygen vacancy occurs simultaneously at the voltage under which the current drops dramatically, indicating that the oxygen vacancy fluctuation also concurs with the resistance state transition. It should be emphasized that the density of oxygen vacancy, whatever in HRS

and LRS, is higher than those in the “forming” process, consisting with the fact that the resistance in the RS behavior is much lower than that in the initial state. Therefore, the experimental results imply strongly that RS behavior of the materials is closely related to the oxygen vacancy generated under the external bias.

Deficiency of oxygen, or generation of oxygen vacancies which act as electron donor dopants, would significantly change the carrier concentration or conductivity of the oxides²⁹. First-principles calculations indicated that the local oxygen reduced area in SrTiO₃ would create a new one-dimensional defect state at the minimum of the conduction band, position the Fermi level in this state and enable electrons to transport, and further reduce the resistance²⁵. Our experimental results support that the RS behavior in this device originates from the local variation of oxygen content. We illustrate

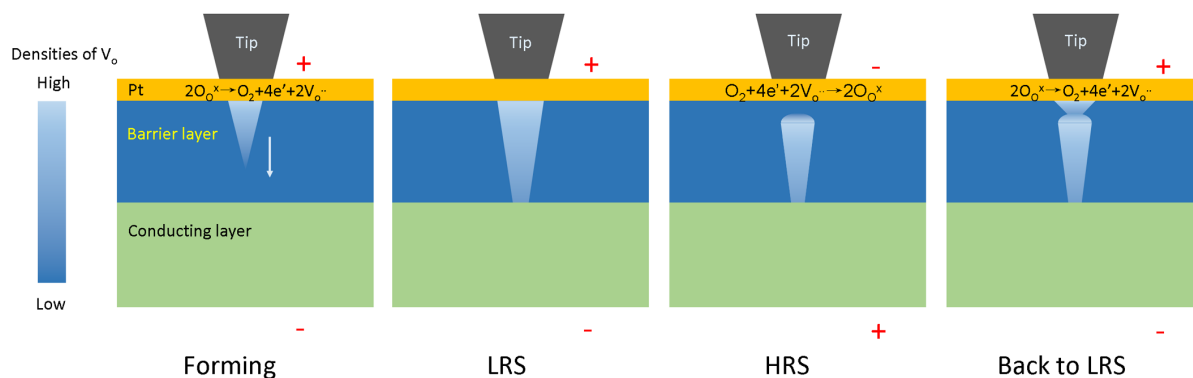


Figure 6 | Schematic diagram of resistance switching of the device. The red symbols “+” and “-” indicate the direction of applied voltage.



a schematic diagram in Fig. 6. When a positive voltage is added, oxygen vacancies should first generate at Pt/LSTO interface and then be repelled towards the cathode, the chemical reaction should be: $2\text{O}_{\text{O}^x} \rightarrow \text{O}_2 + 4e' + 2\text{V}_{\text{O}^{\cdot\cdot}}$, where O_{O^x} means the oxygen in the oxides, and $\text{V}_{\text{O}^{\cdot\cdot}}$ means oxygen vacancy. If the generation of oxygen vacancy is faster than the movement (that depends on the mobility), the density of oxygen vacancies should increase at Pt/LSTO interface, as detected by us, this corresponds to the forming process. When the path of oxygen vacancies penetrates the barrier layer of Pt/LSTO interface, a low resistance state would be achieved. In this state, positive voltage would not influence the resistance obviously. While a negative voltage is added, oxygen vacancies would be vanished at Pt/LSTO as the diagram indicates, the chemical reaction should be: $\text{O}_2 + 4e' + 2\text{V}_{\text{O}^{\cdot\cdot}} \rightarrow 2\text{O}_{\text{O}^x}$. And also because of the mobility, the path would be cut off, the barrier height would be recovered and HRS is represented. Finally, when positive voltage is added again, oxygen vacancies would regenerate at Pt/LSTO interface and reconnect the path in the barrier layer, and thus push the sample back to LRS. Although the relationship between the RS and oxygen content variation is directly confirmed here, the trace of the proposed CFs formed by the oxygen vacancies is still waiting to be investigated in the further research.

In summary, we carried out *in situ* TEM observations for $\text{La}_{0.15}\text{Sr}_{0.85}\text{TiO}_3/\text{SrTiO}_3:\text{Nb}$ with applied electric fields. The RS behavior was observed after the “forming” process by the applied voltage. The EELS characterization for oxygen indicates that the oxygen (vacancy) content correlates closely to the conductivities and RS behavior of our sample. During the “forming” process, the oxygen vacancies generate from the interface of Pt/LSTO by the applied voltage, and the RS behaviors have also a close relationship with the local variation of oxygen content at certain positions after the “forming” process. Our results give direct evidences for the reported mechanism of oxygen vacancy conducting channels for RS behavior, which change the Schottky barrier at the metal/oxide interface, and the *in situ* characterization would be helpful for the further research for the origin of various RS behaviors.

During the *in situ* TEM observation, heating effect by the current passing through the thin TEM lamella is inevitable, and also could induce some deviations, however, we could not estimate the details of heating in this observation by our equipment so far. The effect should be specialized in the further research.

The *in situ* experiments were also realized in scanning TEM (STEM) mode for higher spatial resolution, However, we found that the elemental and time resolutions could not be guaranteed simultaneously, although some corresponding results was indeed found. Considering the data quality, we prefer to present the data in TEM mode in the paper, and put the STEM mode results in the supplementary information (see fig. S2).

Methods

Device fabrication. The sample was fabricated by growing a $\text{La}_{0.10}\text{Sr}_{0.85}\text{TiO}_3$ (LSTO) layer of 1500 Å on a 0.05wt% Nb-doped SrTiO_3 (STON) substrate using the pulsed laser ablation technique. The transport properties of this sample were reported elsewhere²⁸.

TEM sample preparation. To realize an *in situ* observation in TEM, the current has to flow through the thin area of the sample, so we made a tiny fine structure based on the traditional cross-section TEM sample (Fig. 1). The cross-section sample for *in situ* TEM characterization was milled into slice with about 20 μm thick by mechanical polishing, then was stuck on a half Mo grid and fabricated to a thin area for about 200 nm thick by focused ion beam (FIB) technique. At the same time, Pt was deposited on the top of the LSTO as an electrode. An Ar ion-milling process was carried out to the sample after FIB to reduce the Ga-implanted layer. The fabricated sample was connected with a gold wire by silver paste at the STON substrate and equipped in a Nanofactory™ ST-1000 holder. A tungsten probe installed in this holder could touch the Pt electrode. We contact the probe to the thicker part of the specimen to maintain the stability of the tip-sample system, the current density should be equal in the thicker part and the lamella. The schematic diagram of the electric test is shown in Fig. 1.

TEM observations. The TEM observations were performed on a Tecnai F20 microscope equipped with Gatan GIF system. The I-V behavior was measured by the accessories of the Nanofactory™ holder. EELS data were processed with the EELS package in Digital Micrograph.

- Wu, J., Cao, J., Han, W. Q., Janotti, A. & Kim, H. C. *Functional Metal Oxide Nanostructures* (Springer New York, New York, 2012).
- García, V. *et al.* Giant tunnel electroresistance for non-destructive readout of ferroelectric states. *Nature* **460**, 81–84 (2009).
- Akerman, J. Applied Physics: Toward a Universal Memory. *Science* **308**, 508–510 (2005).
- Wuttig, M. & Yamada, N. Phase-change materials for rewriteable data storage. *Nat. Mater.* **6**, 824–832 (2007).
- Waser, R., Dittmann, R., Staikov, G. & Szot, K. Redox-Based Resistive Switching Memories - Nanoionic Mechanisms, Prospects, and Challenges. *Adv. Mater.* **21**, 2632–2663 (2009).
- Ignatiev, A. *et al.* Resistance switching in oxide thin films. *Phase Transitions* **81**, 791–806 (2008).
- Sawa, A. Resistive switching in transition metal oxides. *Mater. Today* **11**, 28–36 (2008).
- Schroeder, H., Pandian, R. & Miao, J. Resistive switching and changes in microstructure. *Phys. Status Solidi A* **208**, 300–316 (2011).
- Kim, K. M., Jeong, D. S. & Hwang, C. S. Nanofilamentary resistive switching in binary oxide system; a review on the present status and outlook. *Nanotechnol.* **22**, 254002 (2011).
- Lamb, D. R. & Rundle, P. C. A non-filamentary switching action in thermally grown silicon dioxide films. *Br. J. Appl. Phys.* **18**, 29 (1967).
- Leon, O. Chua. Memristor-The Missing Circuit Element. *IEEE Trans. Circuit Theory* **5**, 507 (1971).
- Dearnaley, G., Morgan, D. V. & Stoneham, A. M. A Model for Filament Growth and Switching in Amorphous Oxide Films. *J. Non-Cryst. Solids* **4**, 593 (1970).
- Liu, S. Q., Wu, N. J. & Ignatiev, A. Electric-pulse-induced Reversible Resistance Change Effect in Magneto-resistive Films. *Appl. Phys. Lett.* **76**, 2749 (2000).
- Liu, Q. *et al.* Real-Time Observation on Dynamic Growth/Dissolution of Conductive Filaments in Oxide-Electrolyte-Based ReRAM. *Adv. Mater.* **24**, 1844–1849 (2012).
- Yang, Y. *et al.* Observation of conducting filament growth in nanoscale resistive memories. *Nat. Commun.* **3**, 732 (2012).
- Sawa, A., Fujii, T., Kawasaki, M. & Tokura, Y. Hysteretic current-voltage characteristics and resistance switching at a rectifying Ti/Pt_{0.7}Ca_{0.3}MnO₃ interface. *Appl. Phys. Lett.* **85**, 4073 (2004).
- Fujii, T. *et al.* Electrical properties and colossal electroresistance of heteroepitaxial SrRuO₃/SrTi_{1-x}Nb_xO₃ (0.0002 ≤ x ≤ 0.02) Schottky junctions. *Phys. Rev. B* **75**, 165101 (2007).
- Xu, Z.-t. *et al.* Evidence for a Crucial Role Played by Oxygen Vacancies in LaMnO₃ Resistive Switching Memories. *Small* **8**, 1279–1284 (2012).
- Janousch, M. *et al.* Role of Oxygen Vacancies in Cr-Doped SrTiO₃ for Resistance-Change Memory. *Adv. Mater.* **19**, 2232–2235 (2007).
- Jooss, C. *et al.* Polaron melting and ordering as key mechanisms for colossal resistance effects in manganites. *PNAS* **104**, 13597–13602 (2007).
- Rozenberg, M., Inoue, I. & Sánchez, M. Nonvolatile Memory with Multilevel Switching: A Basic Model. *Phys. Rev. Lett.* **92**, 178302 (2004).
- Tokura, Y. *et al.* Filling dependence of electronic properties on the verge of metal–Mott-insulator transition in Sr_{1-x}La_xTiO₃. *Phys. Rev. Lett.* **70**, 2126–2129 (1993).
- Kwon, D.-H. *et al.* Atomic structure of conducting nanofilaments in TiO₂ resistive switching memory. *Nat. Nanotechnol.* **5**, 148–153 (2010).
- In Kyeong, Y. *et al.* Fractal Dimension of Conducting Paths in Nickel Oxide (NiO) Thin Films During Resistance Switching. *IEEE Trans. Nanotechnol.* **9**, 131–133 (2010).
- Szot, K., Speier, W., Bihlmayer, G. & Waser, R. Switching the electrical resistance of individual dislocations in single-crystalline SrTiO₃. *Nat. Mater.* **5**, 312–320 (2006).
- Wang, Z.-H. *et al.* Correlation between evolution of resistive switching and oxygen vacancy configuration in La_{0.5}Ca_{0.5}MnO₃ based memristive devices. *Nanotechnol.* **23**, 265202 (2012).
- Ferreira, P. J., Mitsuishi, K. & Stach, E. A. *In Situ* Transmission Electron Microscopy. *MRS Bull.* **33**, 83–90 (2008).
- Lü, W. M., Sun, J. R., Wang, J. & Shen, B. G. Unusual transport behavior of the SrTiO₃-based homojunctions. *Appl. Phys. Lett.* **95**, 142107–142103 (2009).
- Muller, D. A., Nakagawa, N., Ohtomo, A., Grazul, J. L. & Hwang, H. Y. Atomic-scale imaging of nanoengineered oxygen vacancy profiles in SrTiO₃. *Nature* **430**, 657–661 (2004).
- Zhang, Z., Sigle, W. & Rühle, M. Atomic and electronic characterization of the a[100] dislocation core in SrTiO₃. *Phys. Rev. B* **66**, 094108 (2002).
- Raabe, S. *et al.* *In Situ* Electrochemical Electron Microscopy Study of Oxygen Evolution Activity of Doped Manganite Perovskites. *Adv. Func. Mater.* **22**, 3378–3388 (2012).

Acknowledgments

This work was supported by the State Key Development Program for Basic Research of China (Grant Nos. 2012CB932302 and 2010CB934202), the National Natural Science Foundation of China (Grant No. 10974235).



Author contributions

R.C.Y. designed the experiments and Y.Y. performed the *in situ* TEM experiments, FIB sample fabrication, image processing and data analysis. W.M.L. and J.R.S. fabricated the LSTO/STON sample. Y.Y. and R.C.Y. wrote the paper. Y.Y., J.R.S., C.Z.G., L.G., Y.G.W. and X.F.D. revised the manuscript. All authors discussed the results and commented on the manuscript.

Additional information

Supplementary information accompanies this paper at <http://www.nature.com/scientificreports>

Competing financial interests: The authors declare no competing financial interests.

How to cite this article: Yang, Y. *et al.* *In situ* TEM Observation of Resistance Switching in Titanate Based Device. *Sci. Rep.* 4, 3890; DOI:10.1038/srep03890 (2014).



This work is licensed under a Creative Commons Attribution-NonCommercial-NoDerivs 3.0 Unported license. To view a copy of this license, visit <http://creativecommons.org/licenses/by-nc-nd/3.0>